Supplemental Material for

Projected changes in both mean climate and climate variability drive substantial increases in extreme fire weather in the western United States

Danielle Touma[a,b] & Clara Deser[b]

[a] *Jackson School of Geosciences, Institute for Geophysics, University of Texas at Austin, Austin, TX*

[b] *Climate and Global Dynamics, National Center for Atmospheric Research, Boulder, CO, USA.*

Corresponding author: Danielle Touma, danielle.touma@utexas.edu

Contents of this file

Supplementary Figures S1 to S9

Introduction

The supporting information file includes Figures S1-S9. These supporting figures support the methods, results, and discussion presented in the main manuscript.

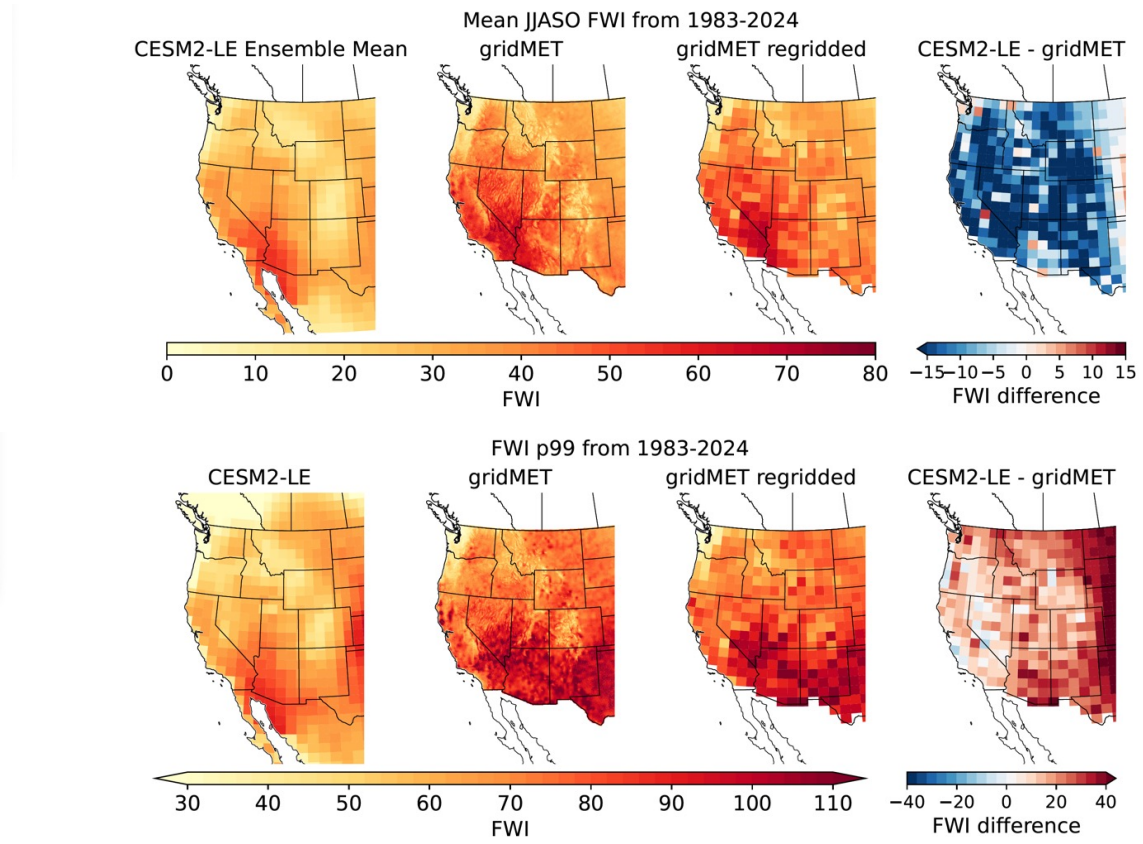

Supplementary Figure 1: Comparison of mean JJASO FWI (top row) and the 99th percentile (bottom row) of FWI from 1983-2024 between CESM2-LE and gridMET (Abatzoglou 2013). To calculate the difference between CESM2-LE and gridMET we regrid the gridMET dataset ("gridMET regridded") to the CESM2-LE grid using bilinear interpolation.

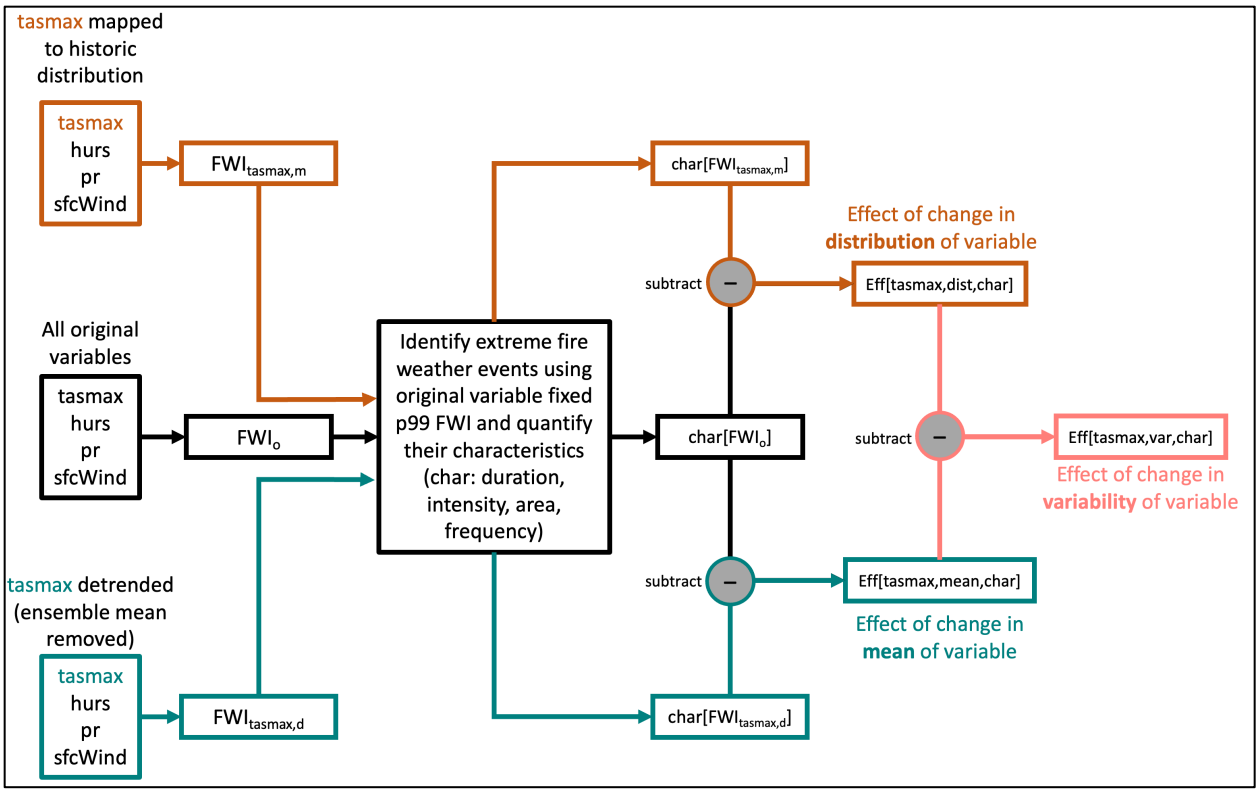

Supplementary Figure 2: Schematic of the calculation of the effect change in distribution, mean, and variability of each variable. In this schematic, the effect of changes in maximum temperature (tasmax) is calculated. *m* is the mapped value, *o* is the original value, and *d*, is the detrended (mean removed) value. *char* is the characteristic of an event (duration, area, frequency, intensity), and *Eff* is the effect of the variable's change (mean, dist, or var) on the characteristic.

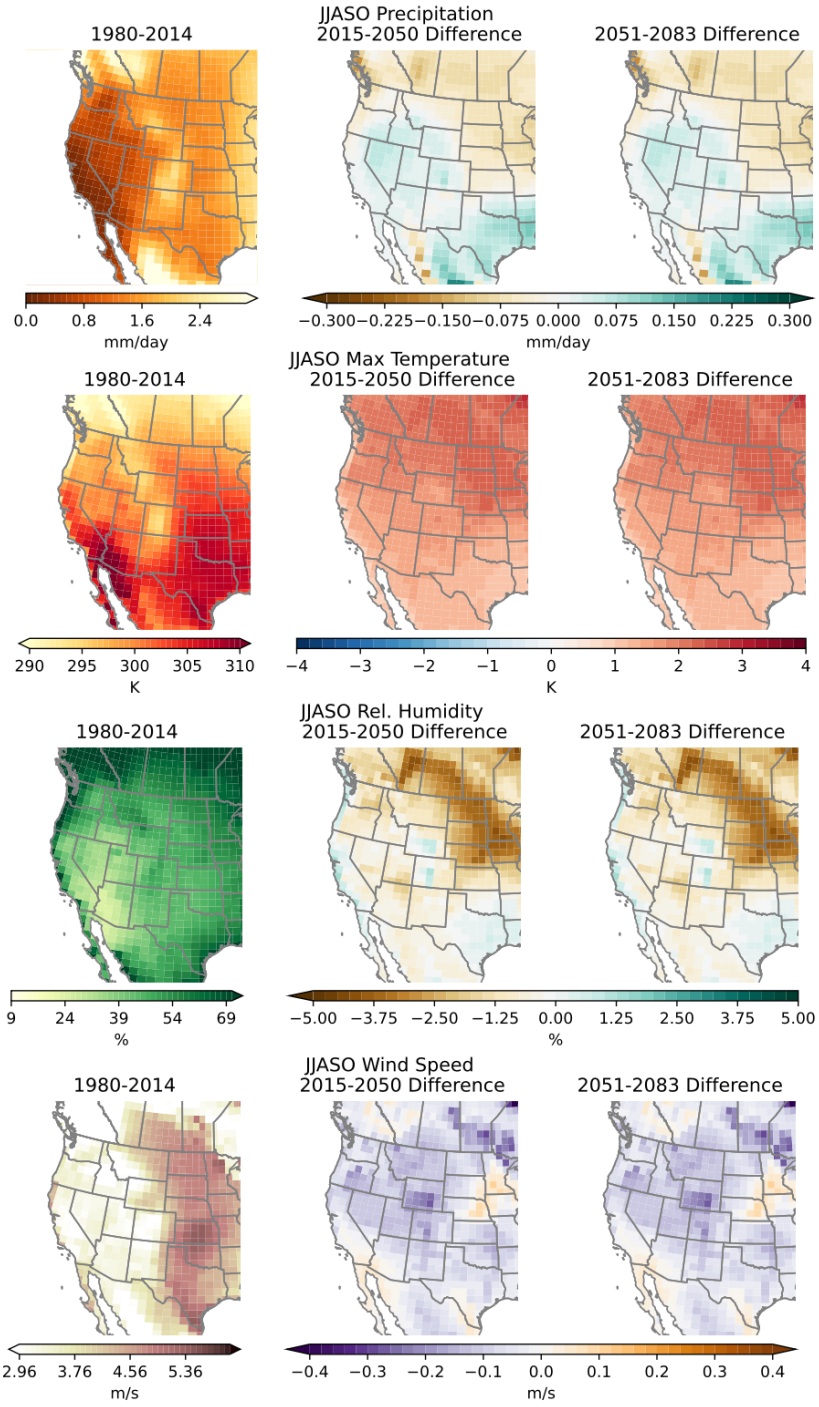

Supplementary Figure 3: Historic mean and future changes in mean precipitation, maximum temperature, relative humidity, and wind speed in JJASO.

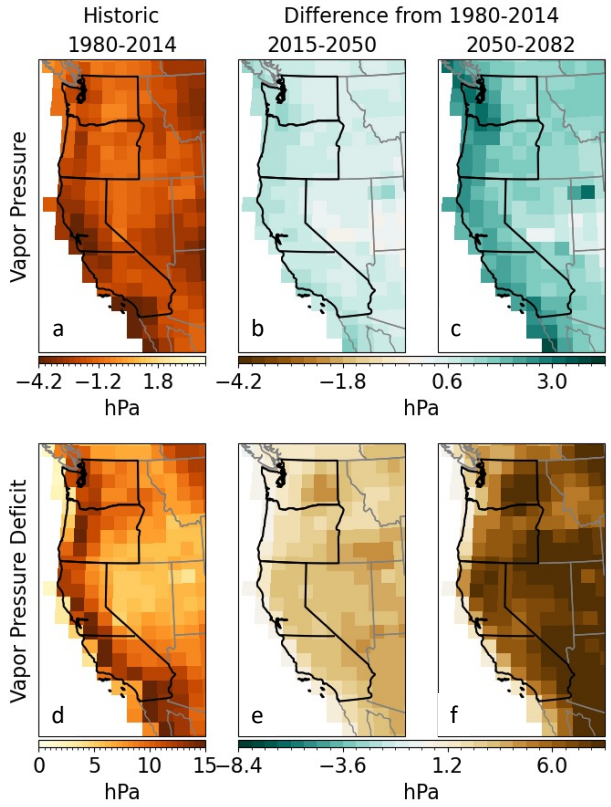

Supplementary Figure 4: Composite maps of vapor pressure (a-c) and vapor pressure deficit (VPD; d-f) during Pacific Coast extreme fire weather events using fixed baseline distributions for calculating FWI thresholds and anomalies.

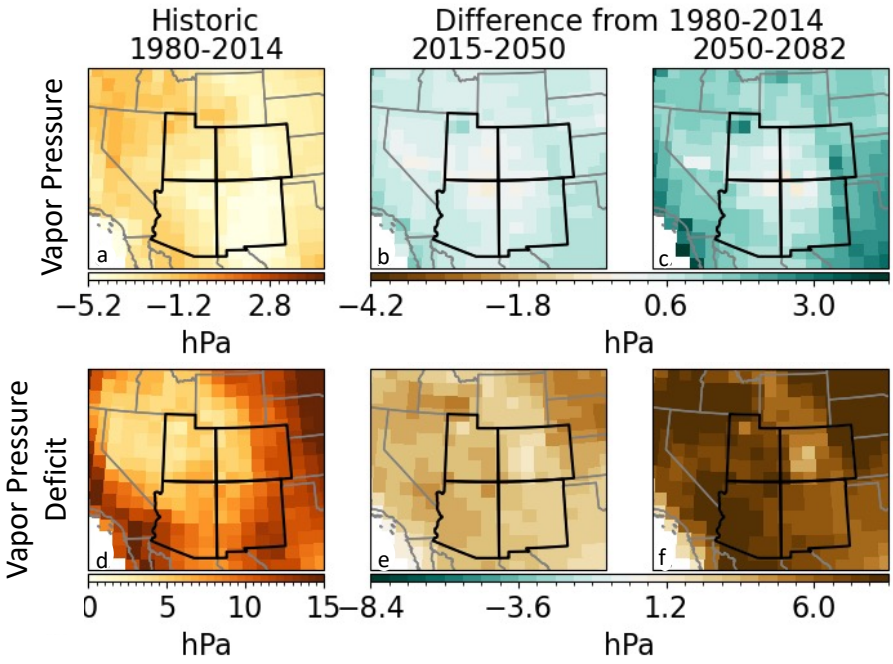

Supplementary Figure 5: Composite maps of vapor pressure (a-c) and vapor pressure deficit (VPD; d-f) during Four Corners extreme fire weather events using fixed baseline distributions for calculating FWI thresholds and anomalies.

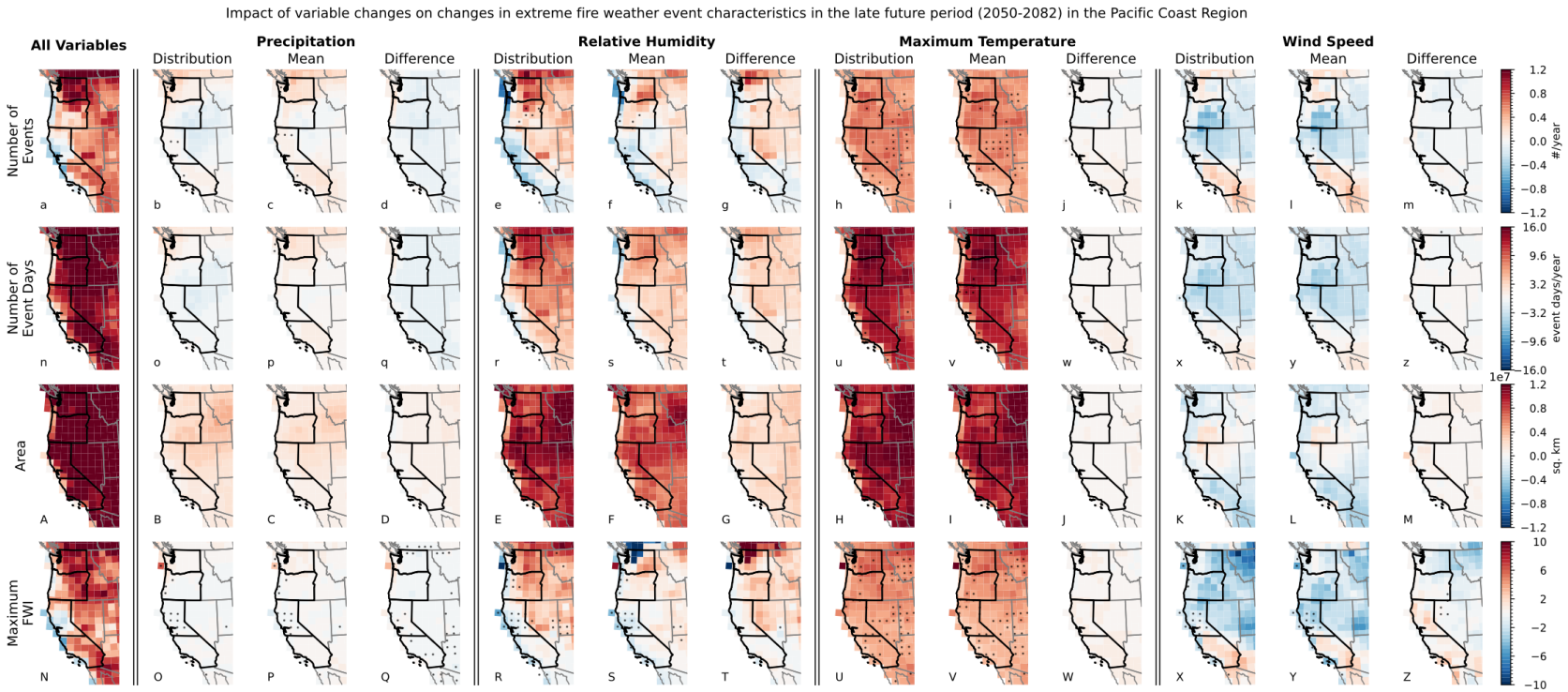

Supplementary Figure 6: The impact of changes in all variables (a, n, A, N), and the full distribution (b, e, h, k, o, r, u, x, B, E, H, K, O, R, U, X), means (c, f, i, l, p, s, v, y, C, F, I, L, P, S, V, Y) and variabilities (s difference ; d, g, j, m, q, t, w, z, D, G, J, M, Q, T, W, Z) of precipitation (b-d, o-q, B-D, O-Q), relative humidity (e-g, r-t, E-G, R-T), maximum temperature (h-j, u-w, H-J, U-W) and wind speed (k-m, x-z, K-M, X-Z) on changes (from the historic period, 1980-2014) in events per year (a-m), events days per year (n-z), event area (A-M), and maximum FWI (N-Z) using the fixed threshold in the late future period (2050-2082) for the Pacific Coast region for JJASO. These composites are created by averaging event characteristics for all events for each ensemble member for each period at each grid point. Then, the grid point-specific values of the historic period are subtracted from each future period for each ensemble member, and the difference values are averaged over all ensemble members.

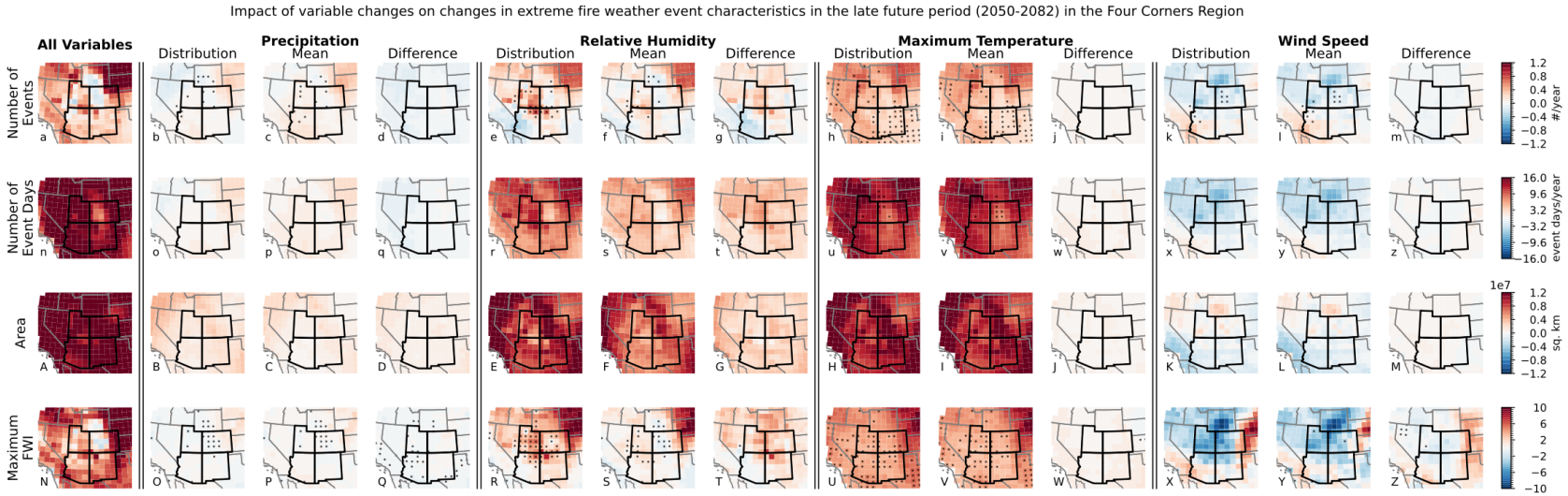

Supplementary Figure 7: The impact of changes in all variables (a, n, A, N), and the full distribution (b, e, h, k, o, r, u, x, B, E, H, K, O, R, U, X), means (c, f, i, l, p, s, v, y, C, F, I, L, P, S, V, Y) and variabilities (s differences ; d, g, j, m, q, t, w, z, D, G, J, M, Q, T, W, Z) of precipitation (b-d, o-q, B-D, O-Q), relative humidity (e-g, r-t, E-G, R-T), maximum temperature (h-j, u-w, H-J, U-W) and wind speed (k-m, x-z, K-M, X-Z) on changes (from the historic period, 1980-2014) in events per year (a-m), events days per year (n-z), event area (A-M), and maximum FWI (N-Z) using the fixed threshold in the late future period (2050-2082) for the Four Corners region for JJASO. These composites are created by averaging event characteristics for all events for each ensemble member for each period at each grid point. Then, the grid point-specific values of the historic period are subtracted from each future period for each ensemble member, and the difference values are averaged over all ensemble members.

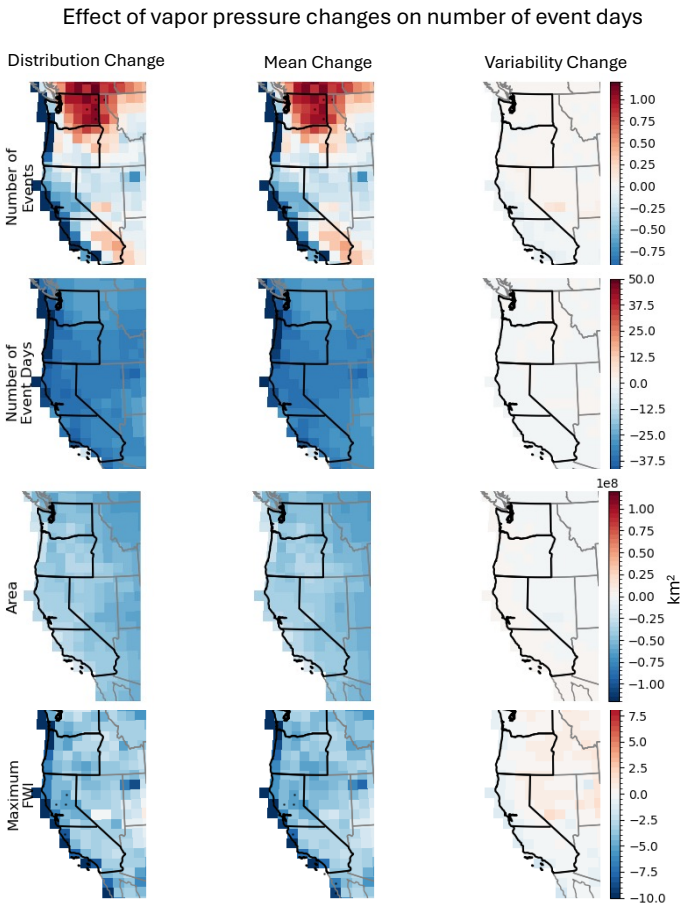

Supplementary Figure 8: The impact of changes in vapor pressure distribution (left column), mean (middle column) and variability (right column) on changes (from the historic period, 1980-2014) in events per year (top row), events days per year (second row), event area (third row), and maximum FWI (last row) using the fixed threshold in the late future period (2050-2082) for the Pacific Coast region for JJASO. The impact of vapor pressure is derived by first using relative humidity and mean temperature to calculate vapor pressure, mapping vapor pressure projections to the historic distribution and mean and then calculating relative humidity using the mapped vapor pressure and original temperature projections. Finally, FWI is recalculated using the mapped relative humidity timeseries and events are identified and characterized. The composites are created by averaging event characteristics for all events for each ensemble member for each period at each grid point. Then, the grid point-specific values of the historic period are subtracted from each future period for each ensemble member, and the difference values are averaged over all ensemble members.

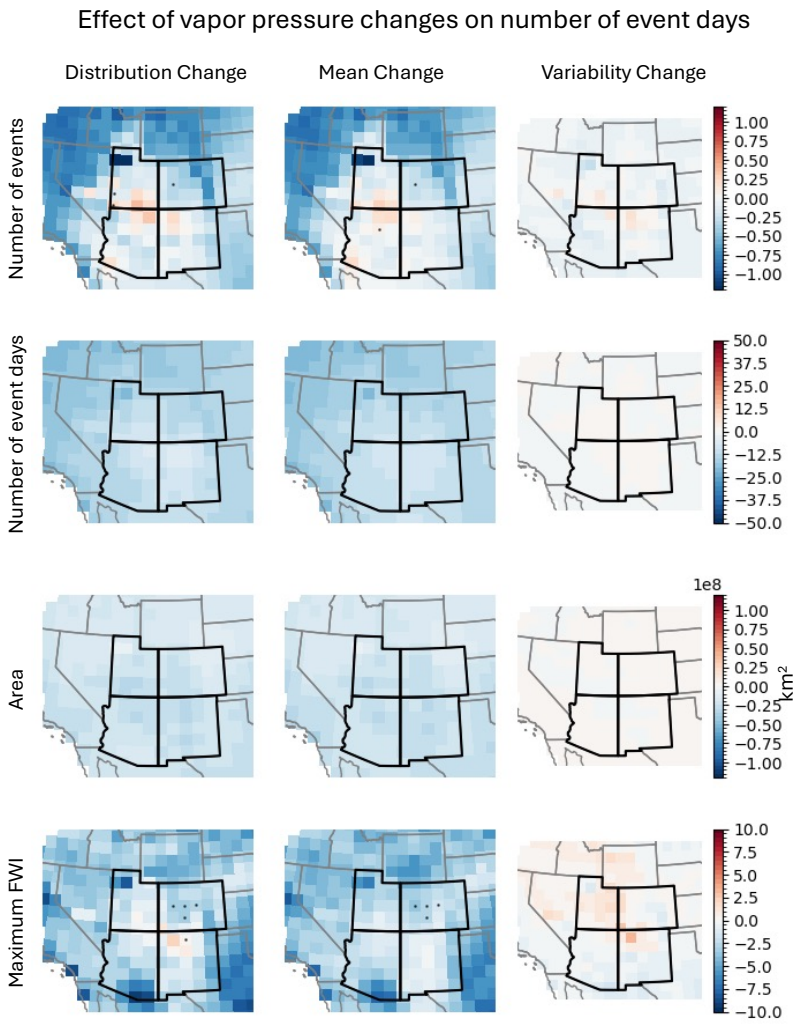

Supplementary Figure 9: The impact of changes in vapor pressure distribution (left column), mean (middle column) and variability (right column) on changes (from the historic period, 1980-2014) in events per year (top row), events days per year (second row), event area (third row), and maximum FWI (last row) using the fixed threshold in the late future period (2050-2082) for the Four Corners region for JJASO. The impact of vapor pressure is derived by first using relative humidity and mean temperature to calculate vapor pressure, mapping vapor pressure projections to the historic distribution and mean and then calculating relative humidity using the mapped vapor pressure and original temperature projections. Finally, FWI is recalculated using the mapped relative humidity timeseries and events are identified and characterized. The composites are created by averaging event characteristics for all events for each ensemble member for each period at each grid point. Then, the grid point-specific values of the historic period are subtracted from each future period for each ensemble member, and the difference values are averaged over all ensemble members.